

Imaging Tumor Metabolism to Assess Disease Progression and Treatment Response

Kerstin N. Timm^{1,2}, Brett W.C. Kennedy^{1,2}, and Kevin M. Brindle^{1,2}

¹Department of Biochemistry, University of Cambridge, Cambridge, United Kingdom

²Cancer Research UK Cambridge Institute, University of Cambridge, Cambridge, United Kingdom

Abstract

Changes in tumor metabolism may accompany disease progression and can occur following treatment, often before there are changes in tumor size. We focus here on imaging methods that can be used to image various aspects of tumor metabolism, with an emphasis on methods that can be used for tumor grading, assessing disease progression, and monitoring treatment response.

Introduction

Reprogramming of metabolism is a recognized hallmark of cancer (1), with altered fluxes in both anabolic and catabolic pathways. Recent work has shown, for example, that some breast cancers are dependent upon increased serine biosynthesis (2) and that human lung tumors show high levels of both glycolysis and glucose oxidation (3). Tumors often preferentially reduce pyruvate to lactate, rather than oxidize it in the tricarboxylic acid (TCA) cycle. This failure to oxidize pyruvate, even in the presence of oxygen (the “Warburg effect”), is not because mitochondria in cancer cells are necessarily dysfunctional, but rather because flux of pyruvate carbon into the TCA cycle is downregulated (4). A major function of the TCA cycle in tumors is to generate building blocks for macromolecular biosynthesis, such as acetyl-CoA for fatty acid synthesis and amino acids for protein synthesis. As in other tissues, tumors can use fuels other than glucose for energy generation, such as glutamine, fatty acids, ketone bodies, and amino acids, with tumors adapting to nutrient availability and other microenvironmental factors (4). Tumor cells can also exist in a metabolic symbiosis, whereby hypoxic tumor cells import glucose and export lactate, while nearby normoxic cells import and catabolize this lactate (5).

Altered metabolic fluxes in cancer cells are intimately linked to control of the redox state. NADPH, which maintains a major cellular antioxidant, glutathione, in a reduced state, can be generated by flux of glutamine carbon through the TCA cycle to malate, with the production of NADPH in the reaction catalyzed by NADP⁺-dependent malic enzyme (ME, EC 1.1.1.40), and by flux of glucose carbon into the pentose phosphate pathway (PPP; ref.

Corresponding Author: Kevin M. Brindle, Cancer Research UK, Cambridge Research Institute, Li Ka Shing Centre, Robinson Way, Cambridge CB2 0RE, United Kingdom. Phone: 4412-2376-9647; Fax: 4412-2376-9510; kmb1001@cam.ac.uk.

Disclosure of Potential Conflicts of Interest

No potential conflicts of interest were disclosed.

4). Decreased glycolytic flux resulting from oxidation of a sensitive sulfhydryl residue in the pyruvate kinase (PK) isoform PKM2 promotes diversion of glucose carbon into the PPP (6). Flux is also diverted into the PPP by TP53-induced glycolysis and apoptosis regulator (TIGAR), which possesses fructose 2,6-bisphosphatase activity and reroutes glycolytic flux into the PPP by decreasing the amount of fructose 2,6-bisphosphate, a potent allosteric activator of the glycolytic enzyme phosphofructokinase 1 (PFK1; ref. 7). Flux of serine and glycine carbon through the tetrahydrofolate (THF) pathway also generates NADPH (2). Increased uptake of glucose and glutamine by cancer cells drives the hexosamine pathway, which yields metabolites involved in protein and lipid glycosylation. Increased *O*-glycosylation of proteins with N-acetylglucosamine promotes cancer cell metabolic reprogramming and cell survival, and sialylation of cell surface carbohydrates is associated with increased metastasis (8).

The differences in metabolism between tumors and normal tissues and the changes in tumor metabolism during disease progression and in response to treatment make metabolic imaging techniques important tools for detecting and grading tumors and for guiding therapy in individual patients (ref. 9; see Fig. 1 and Table 1).

PET

Positron emission tomography (PET) with the glucose analogue 2-[¹⁸F]fluoro-2-deoxy-D-glucose (FDG) is the most widely used metabolic imaging technique in the clinic for tumor staging and assessment of treatment response (10). FDG is trapped by phosphorylation in the reaction catalyzed by the first enzyme in the glycolytic pathway, hexokinase. Many tumor cells overexpress the glucose transporters (GLUT) 1 and 3 and therefore take up large amounts of FDG. However, FDG-PET suffers from a lack of specificity as increased glucose uptake also occurs in inflammation (11). Moreover, sensitivity is low in tumors with a low glycolytic rate, such as prostate tumors, or in tumors that are located in a tissue with high glucose uptake, such as the brain (9). The Royal College of Radiologist's guidelines recommend that imaging tumor treatment response with FDG-PET should commence weeks to months after chemo- or radiotherapy (12), which hampers rapid assessment of a therapy's effectiveness. Recently, a PET tracer for imaging PKM2 expression has been described, ¹¹C]DASA-23, which may be more useful for detecting the increased aerobic glycolytic activity of tumors than FDG. The tracer showed a clear delineation of implanted patient-derived glioblastoma tumors in mouse brain (13). [¹⁸F]-2-deoxy-2-fluoroarabinose has been developed as a potential marker of PPP flux, accumulating predominantly in the liver, where PPP flux is high (14). Most cells take up fatty acids for oxidation and energy production and for biosynthesis of membrane components, but tumors are unusual in that they can derive fatty acids predominantly via *de novo* synthesis (15). However, hypoxic and Ras-transformed cells have been shown to bypass *de novo* lipogenesis by scavenging exogenous fatty acids (16). PET measurements with ¹¹C-acetate have been used to measure *de novo* fatty acid synthesis in a range of cancers (17). ¹¹C-acetate trapped by acetyl-CoA synthetases may also be used for nonlipogenic pathways, such as acetylation of histones (18). In prostate cancer, it is unclear whether ¹¹C-acetate PET adds more clinical information than measurements of prostate-specific antigen (PSA) levels in plasma (19). Glutamine metabolism in many cancers is reprogrammed by oncogenes such as *MYC* and

RAS, redirecting glutamine into biosynthetic pathways to promote proliferation and redox homeostasis, as well as fueling the hexosamine pathway (4). The PET tracer ^{18}F -(2*S*,4*R*)-4-fluoroglutamine (^{18}F -FGln) showed a high tumor-to-brain uptake ratio in glioblastoma-bearing mice as well as in glioblastoma patients with progressive disease (20), which was reduced following the administration of chemo- and radiotherapy in the mice. As there is no uptake in models of neuroinflammation or in mice with a compromised blood–brain barrier, this makes ^{18}F -FGln a specific PET tracer for glutamine-addicted brain tumors. Although a wide range of PET tracers have been developed for interrogating other aspects of tumor metabolism, including tracers that report on uptake of other amino acids and on tissue redox state and pH (19, 21), few have translated into routine clinical practice (21).

A drawback of PET is that only tracer uptake can be assessed, although this may be related to underlying metabolism. Information on true metabolic conversion requires blood sampling to obtain dynamic information on metabolite formation (21). This is not a problem for magnetic resonance spectroscopy (MRS), as the spectrum can identify the observed molecule. For example, glycolytic flux cannot be assessed from PET measurements of FDG uptake, which is an indication of glucose uptake rather than glycolytic flux to pyruvate and lactate. In a study of canine tumors undergoing sequential imaging with hyperpolarized $[1\text{-}^{13}\text{C}]$ pyruvate and FDG PET, there was not always concordance between FDG uptake and $[1\text{-}^{13}\text{C}]$ lactate labeling from hyperpolarized $[1\text{-}^{13}\text{C}]$ pyruvate (22). An advantage of PET, however, is that very low concentrations of tracer can be used, which leaves cell metabolism undisturbed.

MRS

^1H -MRS has been used clinically in the brain, where resonances from choline, lipids, and N-acetylaspartate (NAA) have been observed (23) and in the prostate, where resonances from citrate and choline predominate (24). Metabolite ratios can help define malignant versus benign lesions in both brain and prostate; however, it is questionable how useful these metabolite signals are. ^1H -MRS data can help to identify regions for biopsy, but it is the histopathologic findings rather than MR spectra that guide clinical decision making (25), and in prostate cancer, MRS data add little to multiparametric magnetic resonance imaging (MRI) measurements (26). However, some recently discovered ^1H -MRS biomarkers may be useful. The “oncometabolite” 2-hydroxyglutarate (2HG), which results from a mutation in isocitrate dehydrogenase 1/2 (IDH1/2), can be detected in grade II/III gliomas by ^1H -MRS (27). Although the use of 2HG levels to grade gliomas remains contentious (27), ^1H -MRS measurements of 2HG can also be used to monitor treatment response (28). Glycine may provide another marker of brain tumor malignancy, as the ratio of glycine in tumor versus normal brain increases with glioma grade (29). Germline mutations in the TCA-cycle enzyme succinate dehydrogenase (SDH) can be found in certain renal cancers, pheochromocytomas, gastrointestinal stromal tumors, and paragangliomas. The resulting accumulation of succinate, which can be observed in ^1H spectra (30), may act as an oncometabolite by inhibiting hypoxia-inducible factor 1 (HIF-1) degradation (31).

^{13}C -MRS has been used in clinical studies of brain (32) and lung (3) tumors, where ^{13}C -labeled substrates were infused prior to surgery and tumor samples were frozen immediately

after resection and extracted for ^{13}C -MRS analysis. ^{13}C resonances from glutamine, glutamate, aspartate, γ -aminobutyric acid (GABA), and NAA have been detected in human brain *in vivo* at high magnetic field (7T) following infusion of $[2\text{-}^{13}\text{C}]\text{glucose}$ (33). However, low spatial resolution and long acquisition times would make these ^{13}C -MRS measurements *in vivo* challenging to use in a routine clinical setting.

^{31}P -MRS was used in an early study of a human tumor *in situ* (34); however, a lack of sensitivity has inhibited its use in clinical oncology. The ^{19}F nucleus is almost as sensitive as the proton to NMR detection and has the advantage that there is no background signal in biological systems. ^{19}F -MRS has been used mainly for tracking labeled cells (35) and for detecting probes sensitive to various biologically relevant parameters, such as tumor hypoxia (36). A recent advance is the use of combined PET/MR scanners (37). For example, simultaneous diffusion-weighted MRI and PET measurements of ^{18}F -FDG uptake in both preclinical models and patients (38, 39) allowed metabolic effects to be distinguished from changes in cell viability.

CEST

Metabolites can be detected in MR images of tissue water by exploiting the chemical exchange saturation transfer (CEST) effect. Resonances of labile metabolite protons that exchange with water are selectively saturated using long, low power r.f. pulses, and the resulting decrease in the water signal is detected in a conventional MR image (40). This technique has been used to detect glycogen in mouse liver (41); glucose (gluco-CEST) in tumors, where the signal was shown to correlate with FDG uptake (42); and lactate in a mouse model of lymphoma and in exercising skeletal muscle of healthy volunteers (43). However, in the case of glucoCEST, the contributions of intracellular glucose, glucose metabolites, and glucose in the vasculature and interstitial space to the signal are currently unknown.

Dynamic Nuclear Polarization

Signal from injected ^{13}C -labeled metabolites can be increased greatly ($>10^4 \times$) by dissolution dynamic nuclear polarization (DNP; ref. 44). ^{13}C -labeled molecules are mixed with a stable radical and cooled to approximately 1 K in a high magnetic field. At this temperature, the electron spins in the radical are almost completely polarized. Microwave irradiation at the resonance frequency of the electron spin transfers this polarization to the ^{13}C nuclei. Rapid dissolution with superheated, pressurized buffer brings the ^{13}C -labeled molecule to room temperature with substantial retention of the nuclear spin polarization. The hyperpolarized ^{13}C -labeled substrate can then be injected and the transient hyperpolarized signal, which *in vivo* can last for 2 to 3 minutes depending on the substrate, can be detected using ^{13}C -MRS or ^{13}C magnetic resonance spectroscopic imaging (MRSI; ref. 45). More than 60 hyperpolarized molecules have been used *in vitro* and/or in animal models *in vivo* (46). Hyperpolarized $[1\text{-}^{13}\text{C}]\text{pyruvate}$, which in tumors exchanges the hyperpolarized ^{13}C -label with the large endogenous lactate pool, has transitioned into the clinic. In patients with prostate cancer, hyperpolarized $[1\text{-}^{13}\text{C}]\text{pyruvate}$ allowed early detection of biopsy-proven tumor lesions that were unidentifiable by standard T_2 -weighted MRI (47). Other

metabolites, such as [1,4- $^{13}\text{C}_2$]fumarate (a marker of necrosis; ref. 48) and [1- ^{13}C]dehydroascorbic acid (DHA; a marker of cellular redox state; ref. 49), also show promise for clinical translation (50). Hyperpolarized [U- ^2H , U- ^{13}C]glucose has been used to measure glycolytic flux in a tumor model *in vivo* as well as flux into the PPP (51). Short-chain fatty acid metabolism can be investigated with hyperpolarized [1- ^{13}C]acetate and [1- ^{13}C]butyrate (52, 53), which resulted in the observable labeling of acetylcarnitine in heart muscle. Amino acids have so far shown little promise as hyperpolarized substrates, as their polarization lifetimes are too short to observe slow anabolic processes, and even catabolic processes, such as the deamidation of glutamine, are too slow for MRSI (54).

Hyperpolarized ^{13}C -labeled serine and glycine could, in principle, be used to probe mitochondrial NADPH production via THF metabolism. However, we have not observed metabolism of hyperpolarized ^{13}C -labeled serine or glycine in EL4 murine lymphoma tumors, although small amounts of labeled bicarbonate were produced following injection of hyperpolarized [1- ^{13}C]glycine when data were acquired from over the whole abdomen (unpublished data).

Cytosolic redox state can be assessed by measuring the concentrations of pyruvate and lactate, which are in near equilibrium with NAD^+ and NADH in the reaction catalyzed by lactate dehydrogenase (LDH). Similarly, mitochondrial redox state can be assessed from measurements of the near-equilibrium D-3-hydroxybutyrate/acetoacetate ratio (Fig. 2A). Measurements of the hyperpolarized ^{13}C -labeled lactate/pyruvate ratio in cells incubated with hyperpolarized glucose have been used to estimate the cytosolic NAD^+/NADH ratio (55). However, in a rat Morris hepatocellular carcinoma model, administration of hyperpolarized [1,3- $^{13}\text{C}_2$]ethyl acetoacetate, which was rapidly hydrolyzed by intracellular esterases to produce [1,3- $^{13}\text{C}_2$]acetoacetate, resulted in no detectable production of labeled hydroxybutyrate (56). Addition of hyperpolarized [1,3- $^{13}\text{C}_2$]acetoacetate to an EL4 murine lymphoma cell suspension showed exchange of hyperpolarized ^{13}C label with coinjected unlabeled D-3-hydroxybutyrate, which appeared to be decreased in cells treated with the chemotherapeutic drug etoposide (Fig. 2B and C). This exchange was also observed in implanted EL4 murine lymphoma tumors, without coinjection of unlabeled D-3-hydroxybutyrate. Interestingly, D-3-hydroxybutyrate accumulates in some ovarian cancers (57). In nontumor-bearing mice, ^{13}C label was also observed in acetyl-CoA in the liver/heart region following injection of hyperpolarized [1,3- $^{13}\text{C}_2$]acetoacetate (Fig. 2D). Injection of DL-[1,3- $^{13}\text{C}_2$, 3- ^2H]-3-hydroxybutyric acid into nontumorbearing mice resulted in detectable labeling of acetoacetate, pyruvate, and bicarbonate, when signal was acquired from over the heart/liver region (Fig. 2E; ref. 58).

Current research in this area is focused on improving methods for fast imaging, analyzing kinetic data with [1- ^{13}C]pyruvate, and translating new substrates to the clinic (50). Higher field-strength hyperpolarizers (59) and improved hyperpolarizer designs, with automated injection systems (60), will improve the polarization levels and decrease the transfer time from dissolution to injection. Chemical derivatization to enhance tissue uptake (61) and prolongation of the polarization lifetime by deuteration (51) may allow the use of hyperpolarized substrates that so far have been limited by their slow cell uptake and/or short polarization lifetime. The polarization process, which for a substrate such as

[1-¹³C]pyruvate can take over an hour, can be accelerated by first polarizing protons and then transferring this polarization to the ¹³C nuclei (62).

Imaging Cell Surface Glycosylation

Cell surface glycosylation is important for cell–cell communication and adhesion, and hypersialylation of cell surface glycans confers metastatic potential to a range of cancer cells (8). Glycosylation can be imaged using appropriately labeled probes that bind specific glycan moieties (63). However, probe-based techniques give only a static picture of cell surface glycosylation, whereas metabolic labeling can provide information on glycan turnover. Cell surface glycans can be metabolically labeled with unnatural azido-sugars, and the incorporated sugars can then be reacted *in vivo* with bio-orthogonal probes (64) and visualized, for example, with fluorescence imaging (65), MRI (66), or radionuclide imaging (67). Further development of sensitive radionuclide-labeled probes may allow high-contrast, real-time metabolic imaging of cancer glycosylation *in vivo*, which, in the longer term, has the potential to be translated to the clinic, where it could be used to image cancer progression and assess metastatic potential.

The Future of Metabolic Imaging in Oncology

There are some aspects of tumor metabolism for which there is as yet no imaging probe. Metabolic pathways important for both proliferation and resistance to oxidative stress, such as the PPP and the THF pathway, which produce NADPH, are underexplored imaging targets. Enzymes involved in serine synthesis are emerging drug targets (68), and an imaging technique that could visualize serine/glycine metabolism and one-carbon transfer *in vivo* could improve our understanding of this branch of metabolism. Hyperpolarized [U-²H, U-¹³C]glucose can be used to measure flux through the PPP (51) and may become relevant clinically with improved levels of polarization, potential further increases in polarization lifetime (by selective ¹³C labeling), and by employing routes of administration that allow faster delivery to the tissue of interest. Hyperpolarized [1-¹³C]DHA as a marker of the capability of a tissue to resist oxidative stress (49) also has some potential to reveal new cancer biology. ¹H-MRS can be used to measure oncometabolites, such as 2HG (27) and succinate (30), and the development of hyperpolarized ¹³C-labeled substrates that could be used to explore the pathways leading to these oncometabolites could provide more dynamic information on their metabolism (69). Hyperpolarized DL-[1,3-¹³C₂, 3-²H]-3-hydroxybutyric acid has shown some potential for exploring ketone body metabolism *in vivo* (58). Combining different imaging modalities such as PET/MR (37) with DNP (22) will increase the information content of the imaging examination, allowing more specific information to be obtained from the relatively few metabolic imaging tracers that have been approved for clinical use (70). An emerging health concern in the clinic is the potential toxicity of gadolinium contrast media used in MRI (71). In principle, some of the roles of these contrast media could be replaced with hyperpolarized ¹³C-labeled cell substrates, for example, hyperpolarized ¹³C urea, which has been used to assess tissue perfusion (72). The power of metabolic imaging with hyperpolarized ¹³C-labeled cell substrates is that it gives information on dynamic processes. However, its weakness is that there is no information on the concentrations of the labeled substrates and, therefore, no quantitative information on

flux (expressed, for example, as $M s^{-1}$). Although measurements of changes in this apparent first-order rate constant have been demonstrated to be sufficient to detect treatment response in laboratory-based studies, this will need to be examined carefully in clinical studies. Nevertheless, the technique has great clinical potential for detecting disease, disease progression (73, 74), and treatment response (75) in cancer as well as in other pathologies, such as neurodegenerative disorders and inflammation (50).

Grant Support

The work in K.M. Brindle's laboratory is supported by a Cancer Research UK Programme grant (17242) and the CRUK-EPSRC Imaging Centre in Cambridge and Manchester (16465). Clinical studies are funded by a Strategic Award from the Wellcome Trust (095962). K.N. Timm was in receipt of MRC and Cancer Research UK studentships and B.W.C. Kennedy a Cancer Research UK studentship.

References

1. Hanahan D, Weinberg RA. Hallmarks of cancer: the next generation. *Cell*. 2011; 144:646–74. [PubMed: 21376230]
2. Locasale JW. Serine, glycine and one-carbon units: cancer metabolism in full circle. *Nat Rev Cancer*. 2013; 13:572–83. [PubMed: 23822983]
3. Hensley CT, Faubert B, Yuan Q, Lev-Cohain N, Jin E, Kim J, et al. Metabolic heterogeneity in human lung tumors. *Cell*. 2016; 164:681–94. [PubMed: 26853473]
4. Boroughs LK, DeBerardinis RJ. Metabolic pathways promoting cancer cell survival and growth. *Nat Cell Biol*. 2015; 17:351–9. [PubMed: 25774832]
5. Allen E, Mievillie P, Warren CM, Saghaforia S, Li L, Peng MW, et al. Metabolic symbiosis enables adaptive resistance to anti-angiogenic therapy that is dependent on mTOR signaling. *Cell Rep*. 2016; 15:1144–60. [PubMed: 27134166]
6. Anastasiou D, Poulogiannis G, Asara JM, Boxer MB, Jiang JK, Shen M, et al. Inhibition of pyruvate kinase M2 by reactive oxygen species contributes to cellular antioxidant responses. *Science*. 2011; 334:1278–83. [PubMed: 22052977]
7. Bensaad K, Tsuruta A, Selak MA, Vidal MN, Nakano K, Bartrons R, et al. TIGAR, a p53-inducible regulator of glycolysis and apoptosis. *Cell*. 2006; 126:107–20. [PubMed: 16839880]
8. Pinho SS, Reis CA. Glycosylation in cancer: mechanisms and clinical implications. *Nat Rev Cancer*. 2015; 15:540–55. [PubMed: 26289314]
9. Brindle K. New approaches for imaging tumour responses to treatment. *Nat Rev Cancer*. 2008; 8:94–107. [PubMed: 18202697]
10. Kelloff GJ, Hoffman JM, Johnson B, Scher HI, Siegel BA, Cheng EY, et al. Progress and promise of FDG-PET imaging for cancer patient management and oncologic drug development. *Clin Cancer Res*. 2005; 11:2785–808. [PubMed: 15837727]
11. Zhuang H, Pourdehnad M, Lambright ES, Yamamoto AJ, Lanuti M, Li P, et al. Dual time point 18F-FDG PET imaging for differentiating malignant from inflammatory processes. *J Nucl Med*. 2001; 42:1412–7. [PubMed: 11535734]
12. The Royal College of Radiologists, Royal College of Physicians of London, Royal College of Physicians and Surgeons of Glasgow, Royal College of Physicians of Edinburgh, British Nuclear Medicine Society, Administration of Radioactive Substances Advisory Committee. Evidence-based indications for the use of PET-CT in the United Kingdom 2016. *Clin Radiol*. 2016; 71:e171–88. [PubMed: 27207376]
13. Witney TH, James ML, Shen B, Chang E, Pohling C, Arksey N, et al. PET imaging of tumor glycolysis downstream of hexokinase through noninvasive measurement of pyruvate kinase M2. *Sci Transl Med*. 2015; 7:310ra169. [PubMed: 26491079]
14. Clark PM, Flores G, Evdokimov NM, McCracken MN, Chai T, Nair-Gill E, et al. Positron emission tomography probe demonstrates a striking concentration of ribose salvage in the liver. *Proc Natl Acad Sci U S A*. 2014; 111:E2866–74. [PubMed: 24982199]

15. Menendez JA, Lupu R. Fatty acid synthase and the lipogenic phenotype in cancer pathogenesis. *Nat Rev Cancer*. 2007; 7:763–77. [PubMed: 17882277]
16. Kamphorst JJ, Cross JR, Fan J, de Stanchina E, Mathew R, White EP, et al. Hypoxic and Ras-transformed cells support growth by scavenging unsaturated fatty acids from lysophospholipids. *Proc Natl Acad Sci U S A*. 2013; 110:8882–7. [PubMed: 23671091]
17. Grassi I, Nanni C, Allegri V, Morigi JJ, Montini GC, Castellucci P, et al. The clinical use of PET with (11)C-acetate. *Am J Nucl Med Mol Imaging*. 2012; 2:33–47. [PubMed: 23133801]
18. Comerford SA, Huang Z, Du X, Wang Y, Cai L, Witkiewicz AK, et al. Acetate dependence of tumors. *Cell*. 2014; 159:1591–602. [PubMed: 25525877]
19. Plathow C, Weber WA. Tumor cell metabolism imaging. *J Nucl Med*. 2008; 49:43S–63S. [PubMed: 18523065]
20. Venneti S, Dunphy MP, Zhang H, Pitter KL, Zanzonico P, Campos C, et al. Glutamine-based PET imaging facilitates enhanced metabolic evaluation of gliomas *in vivo*. *Sci Transl Med*. 2015; 7:274ra17. [PubMed: 25673762]
21. Lewis DY, Soloviev D, Brindle KM. Imaging tumor metabolism using positron emission tomography. *Cancer J*. 2015; 21:129–36. [PubMed: 25815854]
22. Gutte H, Hansen AE, Larsen MM, Rahbek S, Henriksen ST, Johannesen HH, et al. Simultaneous hyperpolarized ¹³C-pyruvate MRI and ¹⁸F-FDG PET (HyperPET) in 10 dogs with cancer. *J Nucl Med*. 2015; 56:1786–92. [PubMed: 26338899]
23. Oz G, Alger JR, Barker PB, Barth A, Bizzi A, Boesch C, et al. Clinical proton MR spectroscopy in central nervous system disorders. *Radiology*. 2014; 270:658–79. [PubMed: 24568703]
24. Kobus T, Wright AJ, Scheenen TW, Heerschap A. Mapping of prostate cancer by ¹H MRSI. *NMR Biomed*. 2014; 27:39–52. [PubMed: 23761200]
25. Horska A, Barker PB. Imaging of brain tumors: MR spectroscopy and metabolic imaging. *Neuroimaging Clin N Am*. 2010; 20:293–310. [PubMed: 20708548]
26. Panebianco V, Sciarra A, Marcantonio A, Forte V, Biondi T, Laghi A, et al. Conventional imaging and multiparametric magnetic resonance (MRI, MRS, DWI, MRP) in the diagnosis of prostate cancer. *Q J Nucl Med Mol Imaging*. 2012; 56:331–42. [PubMed: 23013663]
27. de la Fuente MI, Young RJ, Rubel J, Rosenblum M, Tisnado J, Briggs S, et al. Integration of 2-hydroxyglutarate-proton magnetic resonance spectroscopy into clinical practice for disease monitoring in isocitrate dehydrogenase-mutant glioma. *Neuro Oncol*. 2016; 18:283–90. [PubMed: 26691210]
28. Andronesi OC, Loebel F, Bogner W, Marjanska M, Vander Heiden MG, Iafrate AJ, et al. Treatment response assessment in IDH-mutant glioma patients by noninvasive 3D functional spectroscopic mapping of 2-hydroxyglutarate. *Clin Cancer Res*. 2016; 22:1632–41. [PubMed: 26534967]
29. Ganji SK, Maher EA, Choi C. *In vivo* ¹H MRSI of glycine in brain tumors at 3T. *Magn Reson Med*. 2016; 75:52–62. [PubMed: 25651788]
30. Lussey-Lepoutre C, Bellucci A, Morin A, Buffet A, Amar L, Janin M, et al. *In vivo* detection of succinate by magnetic resonance spectroscopy as a hallmark of SDHx mutations in paraganglioma. *Clin Cancer Res*. 2016; 22:1120–9. [PubMed: 26490314]
31. Hirschey MD, DeBerardinis RJ, Diehl AM, Drew JE, Frezza C, Green MF, et al. Dysregulated metabolism contributes to oncogenesis. *Semin Cancer Biol*. 2015; 35:S129–50. [PubMed: 26454069]
32. Mashimo T, Pichumani K, Vemireddy V, Hatanpaa KJ, Singh DK, Sirasanagandla S, et al. Acetate is a bioenergetic substrate for human glioblastoma and brain metastases. *Cell*. 2014; 159:1603–14. [PubMed: 25525878]
33. Li S, An L, Yu S, Ferraris Araneta M, Johnson CS, Wang S, et al. (13) C MRS of human brain at 7 Tesla using [2-(13) C]glucose infusion and low power broadband stochastic proton decoupling. *Magn Reson Med*. 2016; 75:954–61. [PubMed: 25917936]
34. Griffiths JR, Cady E, Edwards RH, McCready VR, Wilkie DR, Wiltshaw E. ³¹P-NMR studies of a human tumour *insitu*. *Lancet*. 1983; 1:1435–6. [PubMed: 6134191]
35. Ahrens ET, Helfer BM, O'Hanlon CF, Schirda C. Clinical cell therapy imaging using a perfluorocarbon tracer and fluorine-19 MRI. *Magn Reson Med*. 2014; 72:1696–701. [PubMed: 25241945]

36. Lee CP, Payne GS, Oregioni A, Ruddle R, Tan S, Raynaud FI, et al. A phase I study of the nitroimidazole hypoxia marker SR4554 using 19F magnetic resonance spectroscopy. *Br J Cancer*. 2009; 101:1860–8. [PubMed: 19935799]
37. Wehrli HF, Sauter AW, Divine MR, Pichler BJ. Combined PET/MR: a technology becomes mature. *J Nucl Med*. 2015; 56:165–8. [PubMed: 25593114]
38. Chen BB, Tien YW, Chang MC, Cheng MF, Chang YT, Wu CH, et al. PET/MRI in pancreatic and perianillary cancer: correlating diffusion-weighted imaging, MR spectroscopy and glucose metabolic activity with clinical stage and prognosis. *Eur J Nucl Med Mol Imaging*. 2016; 43:1753–64. [PubMed: 26993317]
39. Divine MR, Katiyar P, Kohlhofer U, Quintanilla-Martinez L, Pichler BJ, Disselhorst JA. A population-based Gaussian mixture model incorporating 18F-FDG PET and diffusion-weighted MRI quantifies tumor tissue classes. *J Nucl Med*. 2016; 57:473–9. [PubMed: 26659350]
40. van Zijl PC, Yadav NN. Chemical exchange saturation transfer (CEST): what is in a name and what isn't? *Magn Reson Med*. 2011; 65:927–48. [PubMed: 21337419]
41. van Zijl PC, Jones CK, Ren J, Malloy CR, Sherry AD. MRI detection of glycogen *in vivo* by using chemical exchange saturation transfer imaging (glycoCEST). *Proc Natl Acad Sci U S A*. 2007; 104:4359–64. [PubMed: 17360529]
42. Walker-Samuel S, Ramasawmy R, Torrealdea F, Rega M, Rajkumar V, Johnson SP, et al. *In vivo* imaging of glucose uptake and metabolism in tumors. *Nat Med*. 2013; 19:1067–72. [PubMed: 23832090]
43. DeBrosse C, Nanga RP, Bagga P, Nath K, Haris M, Marincola F, et al. Lactate chemical exchange saturation transfer (LATEST) imaging *in vivo* A biomarker for LDH activity. *Sci Rep*. 2016; 6:19517. [PubMed: 26794265]
44. Ardenkjaer-Larsen JH, Golman K, Gram A, Lerche MH, Servin R, Thaning M, et al. Increase of signal-to-noise of more than 10,000 times in liquid state NMR. *Proc Natl Acad Sci U S A*. 2003; 3:37–9.
45. Comment A, Merritt ME. Hyperpolarized magnetic resonance as a sensitive detector of metabolic function. *Biochemistry*. 2014; 53:7333–57. [PubMed: 25369537]
46. Keshari KR, Wilson DM. Chemistry and biochemistry of 13C hyperpolarized magnetic resonance using dynamic nuclear polarization. *Chem Soc Rev*. 2014; 43:1627–59. [PubMed: 24363044]
47. Nelson SJ, Kurhanewicz J, Vigneron DB, Larson PE, Harzstark AL, Ferrone M, et al. Metabolic imaging of patients with prostate cancer using hyperpolarized [1- 13C]pyruvate. *Sci Transl Med*. 2013; 5:198ra08.
48. Gallagher FA, Kettunen MI, Hu DE, Jensen PR, Zandt RI, Karlsson M, et al. Production of hyperpolarized [1,4-13C2]malate from [1,4-13C2]fumarate is a marker of cell necrosis and treatment response in tumors. *Proc Natl Acad Sci U S A*. 2009; 106:19801–6. [PubMed: 19903889]
49. Bohndiek SE, Kettunen MI, Hu DE, Kennedy BW, Boren J, Gallagher FA, et al. Hyperpolarized [1-13C]-ascorbic and dehydroascorbic acid: vitamin C as a probe for imaging redox status *in vivo*. *J Am Chem Soc*. 2011; 133:11795–801. [PubMed: 21692446]
50. Brindle KM. Imaging metabolism with hyperpolarized (13)C-labeled cell substrates. *J Am Chem Soc*. 2015; 137:6418–27. [PubMed: 25950268]
51. Rodrigues TB, Serrao EM, Kennedy BW, Hu DE, Kettunen MI, Brindle KM. Magnetic resonance imaging of tumor glycolysis using hyperpolarized 13C-labeled glucose. *Nat Med*. 2013; 20:93–7. [PubMed: 24317119]
52. Jensen PR, Peitersen T, Karlsson M, In 't Zandt R, Gisselsson A, Hansson G, et al. Tissue-specific short chain fatty acid metabolism and slow metabolic recovery after ischemia from hyperpolarized NMR *in vivo*. *J Biol Chem*. 2009; 284:36077–82. [PubMed: 19861411]
53. Ball DR, Rowlands B, Dodd MS, Le Page L, Ball V, Carr CA, et al. Hyperpolarized butyrate: a metabolic probe of short chain fatty acid metabolism in the heart. *Magn Reson Med*. 2013; 71:1663–9. [PubMed: 23798473]
54. Cabella C, Karlsson M, Canape C, Catanzaro G, Colombo Serra S, Miragoli L, et al. *In vivo* and *in vitro* liver cancer metabolism observed with hyperpolarized [5-C]glutamine. *J Magn Reson*. 2013; 232C:45–52.

55. Christensen CE, Karlsson M, Winther JR, Jensen PR, Lerche MH. Non-invasive in-cell determination of free cytosolic [NAD⁺]/[NADH] ratios using hyperpolarized glucose show large variations in metabolic phenotypes. *J Biol Chem.* 2014; 289:2344–52. [PubMed: 24302737]
56. Jensen PR, Serra SC, Miragoli L, Karlsson M, Cabella C, Poggi L, et al. Hyperpolarized [1,3-¹³C] ethyl acetoacetate is a novel diagnostic metabolic marker of liver cancer. *Int J Cancer.* 2015; 136:E117–26. [PubMed: 25156718]
57. Hilvo M, de Santiago I, Gopalacharyulu P, Schmitt WD, Budczies J, Kuhberg M, et al. Accumulated metabolites of hydroxybutyric acid serve as diagnostic and prognostic biomarkers of ovarian high-grade serous carcinomas. *Cancer Res.* 2016; 76:796–804. [PubMed: 26685161]
58. Kennedy BW, Kettunen MI, Hu DE, Bohndiek SE, Brindle KM. Detection of hyperpolarised ¹³C labeled ketone bodies *in vivo*. *Proc Intl Soc Mag Reson Med.* 2012; 20:4326.
59. Barnes AB, Markhasin E, Daviso E, Michaelis VK, Nanni EA, Jawla SK, et al. Dynamic nuclear polarization at 700 MHz/460 GHz. *J Magn Reson.* 2012; 224:1–7. [PubMed: 23000974]
60. Cheng T, Mishkovsky M, Bastiaansen JA, Ouari O, Hautle P, Tordo P, et al. Automated transfer and injection of hyperpolarized molecules with polarization measurement prior to *in vivo* NMR. *NMR Biomed.* 2013; 26:1582–8. [PubMed: 23893539]
61. Hurd RE, Yen YF, Mayer D, Chen A, Wilson D, Kohler S, et al. Metabolic imaging in the anesthetized rat brain using hyperpolarized [1-¹³C] pyruvate and [1-¹³C] ethyl pyruvate. *Magn Reson Med.* 2010; 63:1137–43. [PubMed: 20432284]
62. Bornet A, Melzi R, Perez Linde AJ, Hautle P, van den Brandt B, Jannin S, et al. Boosting dissolution dynamic nuclear polarization by cross polarization. *J Phys Chem Lett.* 2013; 4:111–4. [PubMed: 26291221]
63. Bird-Lieberman EL, Neves AA, Lao-Sirieix P, O'Donovan M, Novelli M, Lovat LB, et al. Molecular imaging using fluorescent lectins permits rapid endoscopic identification of dysplasia in Barrett's esophagus. *Nat Med.* 2012; 18:315–21. [PubMed: 22245781]
64. Prescher JA, Dube DH, Bertozzi CR. Chemical remodelling of cell surfaces in living animals. *Nature.* 2004; 430:873–7. [PubMed: 15318217]
65. Neves AA, Stockmann H, Wainman YA, Kuo JC, Fawcett S, Leeper FJ, et al. Imaging cell surface glycosylation *in vivo* using “double click” chemistry. *Bioconjug Chem.* 2013; 24:934–41. [PubMed: 23642228]
66. Neves AA, Wainman YA, Wright A, Kettunen MI, Rodrigues TB, McGuire S, et al. Imaging glycosylation *in vivo* by metabolic labeling and magnetic resonance imaging. *Angewandte Chemie.* 2016; 55:1286–90. [PubMed: 26633082]
67. Neves AA, Stockmann H, Harmston RR, Pryor HJ, Alam IS, Ireland-Zecchini H, et al. Imaging sialylated tumor cell glycans *in vivo*. *FASEB J.* 2011; 25:2528–37. [PubMed: 21493886]
68. Pacold ME, Brimacombe KR, Chan SH, Rohde JM, Lewis CA, Swier LJ, et al. A PHGDH inhibitor reveals coordination of serine synthesis and one-carbon unit fate. *Nat Chem Biol.* 2016; 12:452–8.
69. Chaumeil MM, Larson PE, Yoshihara HA, Danforth OM, Vigneron DB, Nelson SJ, et al. Non-invasive *in vivo* assessment of IDH1 mutational status in glioma. *Nat Commun.* 2013; 4:2429.
70. Serrao EM, Brindle KM. Potential clinical roles for metabolic imaging with hyperpolarized [1-(¹³C)]pyruvate. *Front Oncol.* 2016; 6:59. [PubMed: 27014634]
71. Roberts DR, Holden KR. Progressive increase of T1 signal intensity in the dentate nucleus and globus pallidus on unenhanced T1-weighted MR images in the pediatric brain exposed to multiple doses of gadolinium contrast. *Brain Dev.* 2016; 38:331–6. [PubMed: 26345358]
72. von Morze C, Larson PE, Hu S, Yoshihara HA, Bok RA, Goga A, et al. Investigating tumor perfusion and metabolism using multiple hyperpolarized (¹³C) compounds: HP001, pyruvate and urea. *Magn Reson Imaging.* 2012; 30:305–11. [PubMed: 22169407]
73. Albers MJ, Bok R, Chen AP, Cunningham CH, Zierhut ML, Zhang VY, et al. Hyperpolarized ¹³C lactate, pyruvate, and alanine: noninvasive biomarkers for prostate cancer detection and grading. *Cancer Res.* 2008; 68:8607–15. [PubMed: 18922937]
74. Serrao EM, Kettunen MI, Rodrigues TB, Dzien P, Wright AJ, Gopinathan A, et al. MRI with hyperpolarised [1-¹³C]pyruvate detects advanced pancreatic preneoplasia prior to invasive disease in a mouse model. *Gut.* 2016; 65:465–75.

75. Day SE, Kettunen MI, Gallagher FA, Hu DE, Lerche M, Wolber J, et al. Detecting tumor response to treatment using hyperpolarized ^{13}C magnetic resonance imaging and spectroscopy. *Nat Med.* 2007; 13:1382–7. [PubMed: 17965722]



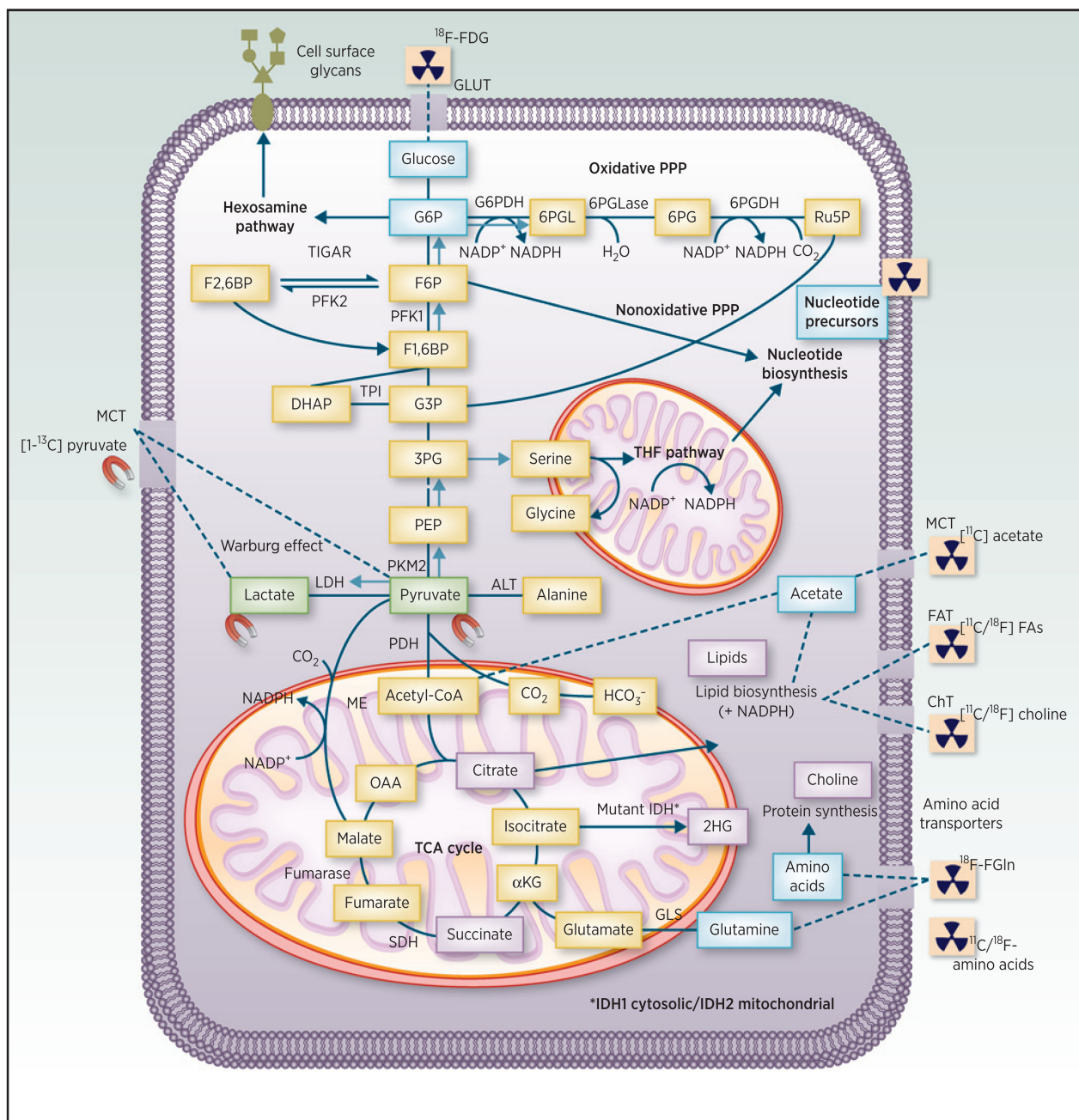


Figure 1.

Clinical imaging of cancer metabolism. Many cancer cells metabolize glucose preferentially to lactate, even in the presence of oxygen (the Warburg effect). Glucose is taken up on the glucose transporters (GLUT), while pyruvate and lactate enter cells through the monocarboxylate transporters (MCT). The PPP is linked to glycolysis via glucose 6-phosphate (G6P), which is oxidized by glucose 6-phosphate dehydrogenase (G6PDH). Flux into the oxidative arm of the PPP is promoted by TIGAR. Serine and glycine can be produced from 3-phosphoglycerate (3PG), and both amino acids can fuel the THF pathway.

Glutamine is deamidated by glutaminase (GLS), which can yield NADPH via NADP⁺-dependent malic enzyme (ME, EC 1.1.1.40) activity. NADPH generated from the oxidative PPP, ME flux, and the THF pathway is used for lipid biosynthesis and redox balance, whereas; intermediates from the nonoxidative PPP and the THF pathway are used for nucleic acid synthesis. Mutant isocitrate dehydrogenase (IDH) in the TCA cycle generates the “oncometabolite” 2-hydroxyglutarate (2HG). IDH1 in the cytosol is mutated in most grade II/III gliomas, whereas IDH2 in the mitochondria is less commonly mutated. The hexosamine pathway branches off from glycolysis at G6P and produces substrates for cell surface glycosylation. Imaging agents that are used clinically and explore some of the aforementioned metabolic features of tumors are shown in blue (PET tracers), green (hyperpolarized substrates), and purple (metabolites detectable by ¹H-MRS). Abbreviations: ¹⁸F-FDG, 2-[¹⁸F]fluoro-2-deoxy-D-glucose; ¹⁸F-FGln, ¹⁸F-(2S,4R)-4-fluoroglutamine; 6PG, 6-phosphogluconate; 6PGDH, 6-phosphogluconate dehydrogenase; 6PGL, 6-phosphogluconolactone; 6PGLase, 6-phosphogluconolactonase; αKG, α-ketoglutarate; ALT, alanine aminotransferase; ChT, choline transporter; DHAP, dihydroxyacetone phosphate; F1,6BP, fructose 1,6-bisphosphate; F2,6BP, fructose 2,6-bisphosphate; FA, fatty acid; G3P, glyceraldehyde 3-phosphate; LDH, lactate dehydrogenase; OAA, oxaloacetate; PEP, phosphoenolpyruvate; PFK1/2, phosphofructokinase 1/2; Ru5P, ribulose 5-phosphate; SDH, succinate dehydrogenase; TPI, triosephosphate isomerase.

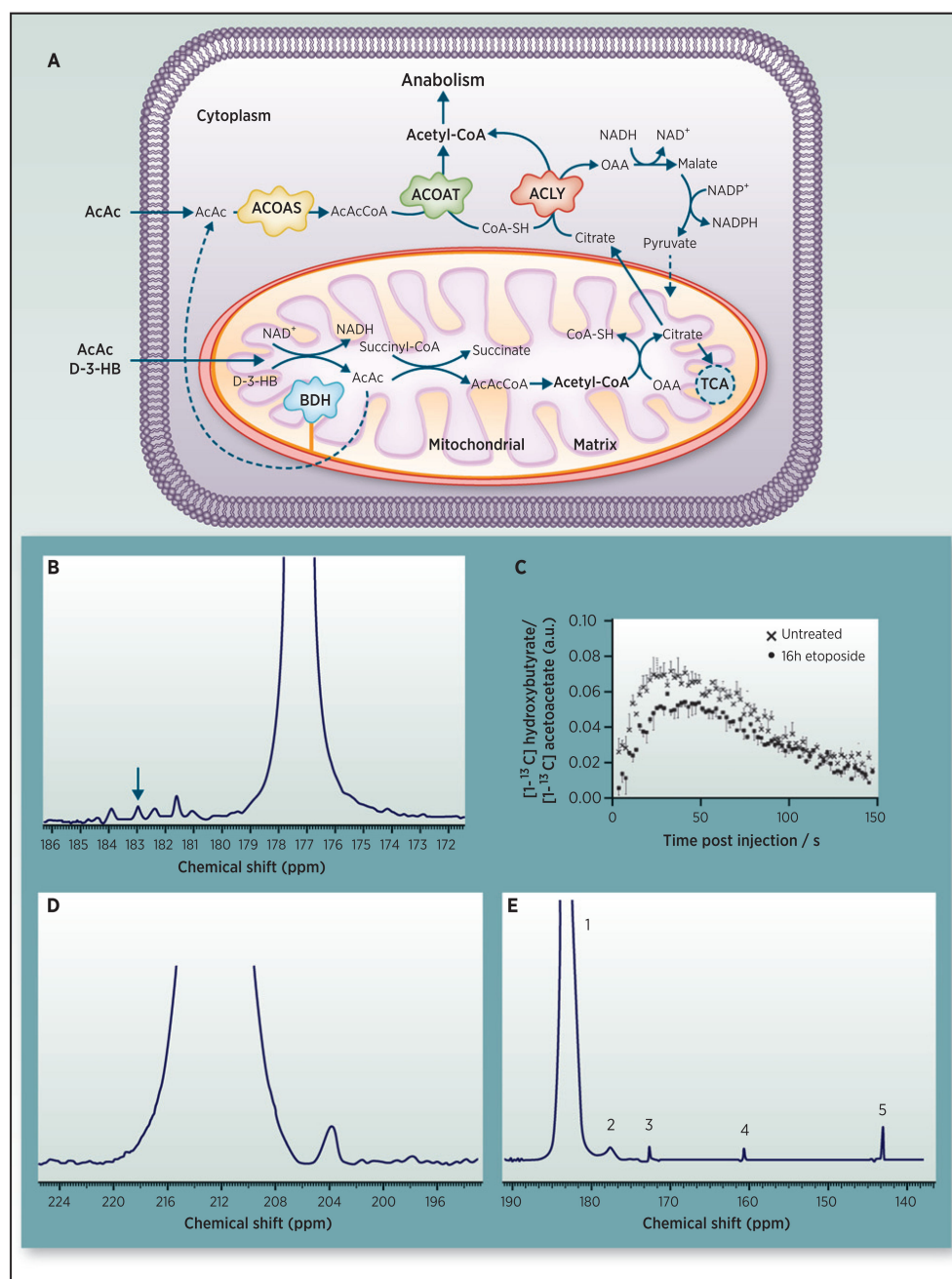


Figure 2.

Assessing ketone body metabolism with hyperpolarized ¹³C-labeled cell substrates. **A**, metabolism of the ketone bodies acetoacetate and D-3-hydroxybutyrate. **B**, spectrum showing the resonances observed 30 seconds after injection of hyperpolarized [1,3-¹³C₂]acetoacetate at a final concentration of 15 mmol/L, into an EL4 murine lymphoma cell suspension (10⁸ cells). Unlabeled D-3-hydroxybutyrate was added in an equimolar amount. There are resonances from C1 [1,3-¹³C₂]acetoacetate at 177.3 ppm and D-3-[1-¹³C]hydroxybutyrate at 183.0 ppm (indicated by the arrow). **C**, labeling of D-3-

hydroxybutyrate decreased after the cells were treated with etoposide for 16 hours (h; unpublished data). **D**, injection of hyperpolarized $[1,3-^{13}\text{C}_2]$ acetoacetate *in vivo*. The spectrum was obtained by summing the first 30 seconds of nonlocalized spectra, where the surface coil was placed directly over the heart/liver region (58). The peak at approximately 212 ppm is C3 $[1,3-^{13}\text{C}_2]$ acetoacetate. The spectrum also shows a resonance at approximately 204 ppm, which is most likely from $[1-^{13}\text{C}]$ acetyl-CoA. **E**, representative spectrum obtained by summing the first 30 seconds of data acquired following administration of 0.2 mL of 60 mmol/L hyperpolarized DL- $[1,3-^{13}\text{C}_2, 3-^2\text{H}]$ -3-hydroxybutyric acid to a nontumor-bearing mouse via a tail vein catheter, where the surface coil was placed directly over the heart/liver region. The observed resonances correspond to: (i) C1 DL-3- $[1,3-^{13}\text{C}_2, 3-^2\text{H}_1]$ hydroxybutyrate (183.0 ppm); (ii) $[1-^{13}\text{C}]$ acetoacetate (177.3 ppm); (iii) $[1-^{13}\text{C}]$ pyruvate (172.8 ppm); (iv) ^{13}C bicarbonate (161.3 ppm); and (v) an unknown metabolite (144.9 ppm; ref. 53). AcAc, acetoacetate; BDH, D-3 hydroxybutyrate dehydrogenase; D-3-HB, D-3-hydroxybutyrate; OAA, oxaloacetate; AcAcCoA, acetoacetyl CoA; ACOAS, acetyl-CoA synthetase; ACOAT, acetyl-CoA thiolase; ACYL, ATP-citrate lyase.

Clinical imaging methods for detecting disease for staging and for assessing treatment response

Table 1

Imaging modality	Tracer	Target	Tumor type	Detection	Staging	Treatment response
PET (12)	2-[¹⁸ F]-fluoro-2-deoxy-D-glucose (FDG)	GLUT1/3, HK	Brain, head and neck, lung, gastrointestinal, esophageal, lymphoma, breast, hepato-pancreato-biliary, urogenital	Yes	Yes	Yes
¹ H-MRS (23,24, 28–30)	¹³ C-acetate	FASN, ACS2, lipid synthesis	HCC	Yes	Yes	
	¹³ C-choline/ ¹⁸ F-fluoro-choline	Cho, ChoK	Prostate, HCC	Yes	Yes	
	⁶⁸ Ga-prostate-specific membrane antigen (PSMA)	PSMA	Prostate	Yes	Yes	
	¹³ C-methionine	LAT1, protein synthesis	Glioma	Yes	Yes	Yes
	¹⁸ F-fluoroethyltyrosine (FET)	LAT1	Glioma	Yes	Yes	Yes
	Endogenous metabolites	NAA	Brain	Yes		
		Lipids	Brain	Yes		
		Choline	Brain, prostate	Yes		
		Citrate	Prostate	Yes		
		2HG	Glioma (clinical trial)	Yes	Yes	Yes
DNP (47)	[1- ¹³ C]pyruvate	Glycine	Glioma (clinical trial)	Yes	Yes	
		Succinate	SDH-mutant paraganglioma	Yes		
		MCT, LDH, [NADH]	Prostate (clinical trial)	Yes		

Abbreviations: 2HG, 2-hydroxyglutarate; ACS2, acyl-CoA synthetase short-chain family member 2; Cho, choline oxidase; ChoK, choline kinase; DNP, dynamic nuclear polarization; FASN, fatty acid synthase; GLUT, glucose transporter; HCC, hepatocellular carcinoma; HK, hexokinase; LAT1, L-type amino acid transporter; LDH, lactate dehydrogenase; MCT, monocarboxylate transporter; MRS, magnetic resonance spectroscopy; NAA, N-acetylaspartate; PET, positron emission tomography; SDH, succinate dehydrogenase.